

The absorption line spectrum of J2233–606

P. J. Outram¹, B. J. Boyle², R. F. Carswell¹, P. C. Hewett¹,
R. E. Williams³, R. P. Norris⁴

¹ *Institute of Astronomy, Madingley Road, Cambridge CB3 0HA*

² *Anglo-Australian Observatory, PO Box 296, Epping, NSW 2121, Australia*

³ *Space Telescope Science Institute, 3700 San Martin Drive, Baltimore, MD 21218 USA*

⁴ *Australia Telescope National Facility, Epping, NSW 2121, Australia*

13 September 2018

ABSTRACT

We report on high resolution observations ($R = 35000$) of the Hubble Deep Field South QSO J2233-606 obtained with the University College London Echelle Spectrograph at the AAT. We present spectral data and an associated absorption line list for the wavelength region $3530 < \lambda < 4390 \text{ \AA}$. The data has a mean signal-to-noise ratio in the continuum of approximately 15 per 0.05 \AA resolution element at $\lambda > 3700 \text{ \AA}$.

Key words: quasars: absorption line systems – quasars: individual : J2233-606

1 INTRODUCTION

The Hubble Deep Field (Williams et al. 1996) provided unprecedented information on the nature of the Universe at high redshifts (e.g. Abraham et al. 1996, Steidel et al. 1996, Madau et al. 1996). A similar study of a southern field in the HST continuous viewing zone has just been completed. A primary goal of the Hubble Deep Field South (HDF-S) project will be to further our understanding of the relationship between galaxies and quasar absorption line systems and the HST field will be centred on a bright high-redshift quasar. The position of the HDF-S field was determined by the location of the bright ($B = 17.5$) $z = 2.24$ QSO J2233–606, discovered by one of us (PCH) and M J Irwin using APM scans of a UKST objective-prism plate, with confirmation of the object by the AAT (Boyle 1997).

The main reasons for centring the HDF-S on a high redshift quasar are to compare the absorption line spectrum of the quasar with the redshifts of the galaxies identified in the field, and to probe the quasar environment.

Initial spectral observations of J2233–606 have already been reported by Sealey, Webb & Drinkwater (1998) and Savaglio (1998). Sealey et al. (1998) combined observations made with the ANU 2.3m telescope with HST STIS observations to yield a low resolution spectrum ($R = 5000$) over the wide wavelength range $2000 < \lambda < 8000 \text{ \AA}$. Savaglio (1998) reported on intermediate-resolution ($R = 11000$) observations obtained with the EMMI spectrograph on the ESO 3.6m telescope in the wavelength region $4500 < \lambda < 8200 \text{ \AA}$.

In this paper we report on high-resolution observations ($R \sim 35000$) of J2233–606 made with the University College of London Echelle Spectrograph (UCLES) at the Anglo-Australian Telescope (AAT). These observations cover the important wavelength region $3530 < \lambda < 4390 \text{ \AA}$, compris-

ing much of the key Ly α forest region. This data also largely bridges the gap between the HST STIS ($\lambda < 3500 \text{ \AA}$) observations and the existing EMMI observations ($\lambda > 4400 \text{ \AA}$) providing nearly contiguous spectral coverage at resolution of at least $R = 10000$ over the full wavelength range $1150 \text{ \AA} < \lambda < 8200 \text{ \AA}$.

2 OBSERVATIONS

Observations of J2233–606 were made with UCLES on three separate observing runs: 1997 August 24–25, 1998 July 28–31 and 1998 August 17–19. Details are given in table 1. The first and third of these runs were both carried out with the 31 line mm^{-1} cross-dispersing grating and the 1024² Tektronix CCD. The 31 line mm^{-1} grating gives a smaller spacing between the orders on the echellogram (and thus greater wavelength coverage for a given detector size), but at the expense of a smaller slit length (8 arcsec). The Tektronix chip was binned by a factor of two in the spatial direction for readout, giving a spatial resolution of $0.7 \text{ arcsec pixel}^{-1}$. The chip was readout in XTRASLOW mode, with a readnoise of 2.3 electrons. Unless interrupted by poor weather, integrations on the QSO were split into exposures of 3600 seconds, representing a compromise between short exposures dominated by read noise and long exposures dominated by cosmic rays events. The spectral resolution provided by the Tektronix CCD is $\sim 0.04 \text{ \AA pixel}^{-1}$. The slit-widths used throughout the August 1997 and August 1998 observations (1.2–1.4 arcsec) project to between 2.7 and 3.2 pixels on this detector.

Good seeing (1.5 arcsec or less) and photometric conditions were obtained on three out of the five nights with the Tektronix CCD/31 line mm^{-1} grating (see table 1). This resulted in almost 100000 seconds integration being

Table 1. Details of Observations

Date	Wavelength Range	Grism/CCD	Photometric	Seeing	Exposure
1997 August 24	3353–3989Å	31/Tek	No	2.0–2.5	18000 sec
1997 August 25	3353–3989Å	31/Tek	Yes	1.0–1.2	25200 sec
1998 July 31	3319–4075Å	79/MITLL	No	2.5–4.0	19800 sec
1998 August 17	3557–4392Å	31/Tek	No	1.2–1.4	22200 sec
1998 August 18	3557–4392Å	31/Tek	Yes	1.2–1.5	36000 sec
1998 August 19	3557–4392Å	31/Tek	Yes	1.4–1.5	28800 sec

obtained in good conditions over the key spectral region $3560 < \lambda < 3990\text{\AA}$, covering the Ly α emission line and a significant fraction of the Ly α forest. In addition, over 70000 seconds integration was achieved in similar conditions over wavelength region $3990 < \lambda < 4360\text{\AA}$ immediately to the red of the Ly α emission line. Further observations were made in more marginal conditions.

Unfortunately, we were unable to extend observations to the blue wavelength limit of the Savaglio observations at $\sim 4400\text{\AA}$ at appreciable signal-to-noise ratio (S/N). The reddest UCLES order lay right on the edge of the Tektronix chip ($4360 < \lambda < 4394\text{\AA}$), making sky subtraction very difficult. We were, however, able to extract it with much higher noise levels.

The 1998 July observations were carried out with the 79 line mm^{-1} grating and a lumogen-coated 4096×2048 MIT/Lincoln Labs CCD. Compared to the Tektronix CCD, the MIT/LL CCD has a significantly lower read noise (1.4 electrons in SLOW mode), is less affected by cosmic rays, and has a larger area covering more of the echellogram. Unfortunately much of this additional area is severely vignetting (up to 50 per cent) by the existing UCLES camera. A more serious disadvantage of the MIT/LL CCD is its much lower quantum efficiency (35 per cent) than the Tektronix CCD (40–60 per cent) in the region 3700–5000Å, which comprises most of the wavelengths of interest here. However, it was decided to attempt one set of observations with this chip to obtain good coverage down in the range 3350–3500Å, where the quantum efficiency of the lumogen-coated MIT/LL CCD remains constant at 35 per cent, and is, consequently, much higher than that of the Tektronix CCD. Unfortunately the weather during the July 1998 run was very poor indeed, only 5 hours observations were possible, all in poor seeing (> 2.5 arcsec). These observations have been added into the final spectrum reproduced below, with appropriate weights, but provide little additional data.

3 DATA REDUCTION

Standard IRAF packages were used to process the raw images, applying bias and flat-field corrections. The cosmic rays were flagged using a median filter and given zero weight in the individual frames. The sky-subtracted spectra were then optimally extracted, along with a one-sigma error estimate. Calibration to vacuum heliocentric wavelengths was obtained using spectra from a Thorium-Argon lamp. The standard star EG274 was used for flux calibration. The echelle orders were then resampled to the same dispersion, and added together weighted according to their S/N. The final spectrum, with a spectral range $3529 < \lambda < 4394$, is

shown in figure 1. It has a resolution, measured from the lamp emission lines, of 8.5 km s^{-1} full width half maximum (FWHM) and a typical S/N per 0.05 bin of ~ 15 in the Ly α forest region, and ~ 20 long-ward of the Ly α emission.

Voigt Profiles were fitted, using a χ^2 minimization technique, to the absorption features in order to determine the redshifts, column densities and Doppler widths of ions identified with observed absorption lines. A more complete description of the fitting procedure, using the software package VPFIT (Webb 1987; Carswell et al. 1992), can be found in Outram, Chaffee & Carswell (1998).

Heavy element lines identified within the Ly α forest are either in systems which show features longward of the Ly α emission line, or were found by looking for common doublets such as C IV $\lambda\lambda 1548, 1550$, Si IV $\lambda\lambda 1393, 1402$, or Mg II $\lambda\lambda 2796, 2803$.

4 RESULTS

We present the absorption line parameter fits in table 2. A total of 10 heavy element systems, as well as 89 Ly α forest lines were seen in the spectrum. The HI column density limit in the forest is set mainly by continuum uncertainties, and varies with S/N. On average the limit is $\log N(\text{H I}) \sim 13$ for a Doppler parameter of 20 km s^{-1} , corresponding to an equivalent width limit of $\sim 25 \text{ mÅ}$.

4.1 The Ly α Forest

We have obtained spectral coverage of the Ly α forest over the wavelength region $3530 < \lambda < 3950\text{\AA}$, corresponding to a redshifts from $z = 1.9$ to the emission redshift of the quasar, $z = 2.24$. The S/N per 0.05\AA bin falls off at shorter wavelengths, dropping gradually from ~ 30 on the Ly α emission peak, to approximately six at $\lambda = 3600\text{\AA}$. Below $\lambda = 3550\text{\AA}$ the S/N drops dramatically to around three, because this region was not covered in the August 1998 run. It was included, however, because of the important Si III lines corresponding to the $z = 1.92$ and $z = 1.94$ systems. No other Ly α lines were detected here.

A total of 89 Ly α lines were fitted. The parameter distributions follow a similar pattern to that seen in other quasar spectra (e.g. Lu et al. 1996; Kirkman & Tytler 1997). The H I column density distribution, for $13.3 < \log N < 16$, is consistent with a power law distribution of slope -1.5 . The Doppler parameter distribution is well described by a Gaussian of mean $b = 25 \text{ km s}^{-1}$, $\sigma_b = 15 \text{ km s}^{-1}$, and a cut-off below $b = 18 \text{ km s}^{-1}$. About 8 per cent of the Ly α lines have Doppler widths smaller than this, but this could be due to either contamination of the sample by narrower unidentified

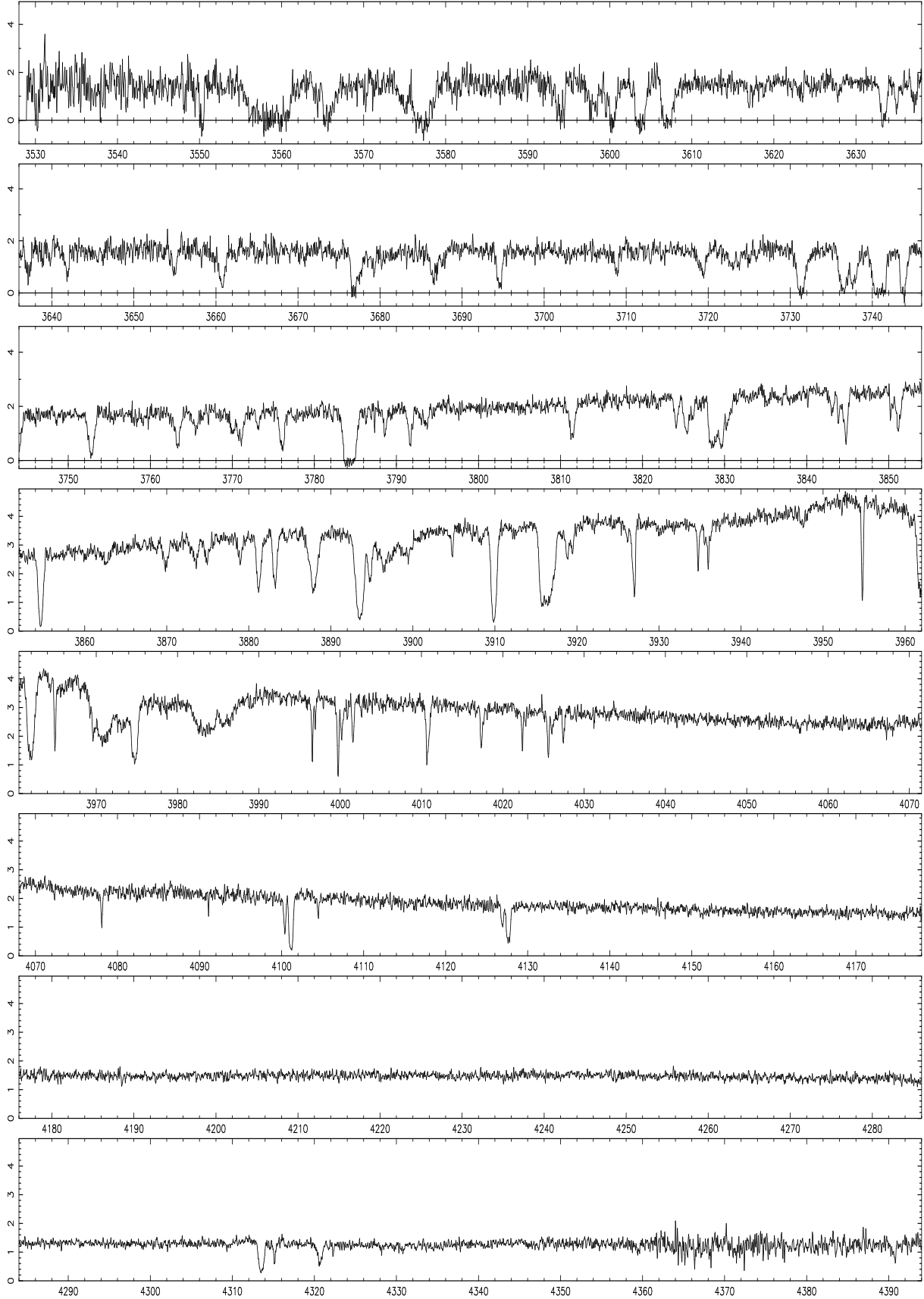


Figure 1. The spectrum of J2233–606, plotted against vacuum heliocentric wavelength(Å).

Table 2. Absorption line parameter list

ID	λ_{rest}	λ_{obs}	z	σ_z	b	σ_b	LogN	σ_{LogN}
Si III	1206.50	3529.85	1.925698	0.000017	14.73	2.37	12.359	0.357
Si III	1206.50	3530.18	1.925971	0.000003	6.75	0.37	13.300	0.483
Si III	1206.50	3549.49	1.941975	0.000003	11.49	0.64	12.362	0.424
Si III	1206.50	3550.05	1.942434	0.000005	10.71	0.67	13.039	0.258
Si III	1206.50	3550.26	1.942610	0.000002	6.42	0.34	14.988	0.478
H I	1215.67	3556.33	1.925409	0.000054	53.28	7.04	14.148	0.071
H I	1215.67	3558.16	1.926913	0.000027	30.44	3.99	17.780	0.845
H I	1215.67	3560.23	1.928615	0.000027	40.78	5.68	14.887	0.246
H I	1215.67	3565.69	1.933103	0.000027	59.33	3.70	14.276	0.042
H I	1215.67	3570.20	1.936817	0.000034	20.03	4.81	13.194	0.095
H I	1215.67	3574.59	1.940430	0.000187	43.99	18.38	13.498	0.233
H I	1215.67	3575.10	1.940845	0.000028	16.47	5.49	13.493	0.200
H I	1215.67	3577.02	1.942429	0.000018	23.44	0.92	18.205	0.099
H I	1215.67	3578.45	1.943607	0.000036	19.38	5.33	13.360	0.119
H I	1215.67	3581.13	1.945809	0.000103	44.23	15.49	13.128	0.142
H I	1215.67	3593.20	1.955738	0.000440	38.93	38.92	13.137	0.633
H I	1215.67	3593.98	1.956380	0.000064	33.97	6.00	14.007	0.100
H I	1215.67	3597.95	1.959642	0.000033	56.65	4.62	13.930	0.038
H I	1215.67	3600.19	1.961487	0.000021	46.16	2.99	14.197	0.045
H I	1215.67	3603.71	1.964382	0.000014	33.42	3.07	14.820	0.195
H I	1215.67	3607.05	1.967126	0.000016	42.40	3.10	14.641	0.115
H I	1215.67	3616.94	1.975263	0.000012	10.62	1.66	13.285	0.071
H I	1215.67	3623.22	1.980434	0.000042	29.53	6.16	13.094	0.081
H I	1215.67	3627.82	1.984215	0.000035	28.02	4.95	13.175	0.069
H I	1215.67	3633.34	1.988755	0.000011	28.17	1.78	14.175	0.065
H I	1215.67	3634.94	1.990068	0.000014	20.30	1.88	13.529	0.042
H I	1215.67	3637.11	1.991857	0.000019	25.34	2.53	13.511	0.043
H I	1215.67	3641.82	1.995729	0.000015	18.05	2.03	13.322	0.046
H I	1215.67	3654.90	2.006494	0.000022	28.39	2.93	13.462	0.043
H I	1215.67	3659.74	2.010472	0.000064	32.16	9.31	13.100	0.107
H I	1215.67	3660.74	2.011293	0.000018	31.05	2.47	13.860	0.036
H I	1215.67	3670.80	2.019568	0.000019	9.37	2.80	12.741	0.102
H I	1215.67	3676.76	2.024476	0.000018	19.30	2.40	14.217	0.143
H I	1215.67	3677.39	2.024992	0.000097	41.32	8.95	13.689	0.114
H I	1215.67	3678.59	2.025979	0.000023	10.74	3.53	12.717	0.112
H I	1215.67	3679.21	2.026488	0.000019	20.07	2.73	13.236	0.052
H I	1215.67	3686.52	2.032498	0.000024	41.26	3.32	13.733	0.031
H I	1215.67	3687.61	2.033399	0.000048	25.94	6.88	12.971	0.101
H I	1215.67	3694.53	2.039087	0.000010	24.44	1.31	13.826	0.032
Si II	1260.42	3708.71	1.942434	0.000005	10.71	0.67	12.577	0.067
Si II	1260.42	3708.93	1.942610	0.000002	6.42	0.34	12.524	0.073
H I	1215.67	3731.28	2.069322	0.000012	28.55	2.34	14.234	0.069
H I	1215.67	3731.57	2.069556	0.000067	85.86	9.48	13.694	0.068
H I	1215.67	3736.45	2.073570	0.000013	35.52	1.72	14.140	0.028
H I	1215.67	3737.66	2.074572	0.000018	39.47	2.71	13.880	0.027
H I	1215.67	3740.23	2.076684	0.000923	109.04	56.41	13.559	0.496
H I	1215.67	3740.83	2.077173	0.000011	33.08	3.46	15.400	0.255
H I	1215.67	3742.36	2.078432	0.000272	37.21	29.70	12.785	0.672
H I	1215.67	3743.75	2.079577	0.000007	24.78	1.19	14.211	0.051
H I	1215.67	3752.79	2.087013	0.000008	30.05	1.07	13.894	0.021
H I	1215.67	3758.69	2.091871	0.000074	75.92	11.84	13.233	0.073
H I	1215.67	3763.27	2.095634	0.000011	29.43	1.34	13.613	0.020
H I	1215.67	3765.50	2.097465	0.000022	31.02	2.96	13.202	0.037
H I	1215.67	3769.99	2.101162	0.000022	26.94	2.99	13.273	0.042
H I	1215.67	3770.95	2.101952	0.000017	34.09	2.38	13.584	0.025
H I	1215.67	3773.12	2.103734	0.000017	19.84	2.25	13.053	0.043
H I	1215.67	3776.04	2.106139	0.000009	26.24	1.09	13.688	0.020
H I	1215.67	3784.29	2.112923	0.000007	43.05	1.35	14.800	0.059
H I	1215.67	3788.59	2.116465	0.000011	17.33	1.40	13.192	0.032
H I	1215.67	3791.63	2.118963	0.000009	22.18	1.14	13.476	0.022
H I	1215.67	3793.45	2.120458	0.000036	53.52	4.73	13.313	0.034
H I	1215.67	3811.37	2.135201	0.000009	30.67	1.17	13.550	0.016
H I	1215.67	3824.09	2.145662	0.000009	20.59	1.20	13.208	0.022

Table 2. Absorption line parameter list

ID	λ_{rest}	λ_{obs}	z	σ_z	b	σ_b	LogN	σ_{LogN}
H I	1215.67	3825.34	2.146696	0.000010	30.52	1.40	13.523	0.016
H I	1215.67	3826.10	2.147319	0.000012	15.67	1.78	12.965	0.043
H I	1215.67	3826.96	2.148028	0.000034	32.62	5.21	12.866	0.055
H I	1215.67	3828.30	2.149128	0.000071	24.79	6.66	13.591	0.492
H I	1215.67	3828.86	2.149590	0.000191	39.99	28.86	13.803	0.370
H I	1215.67	3829.58	2.150181	0.000017	18.35	2.53	13.588	0.124
H I	1215.67	3830.27	2.150747	0.000038	44.44	4.12	13.517	0.040
H I	1215.67	3835.20	2.154801	0.000029	19.23	4.18	12.613	0.083
Si II	1304.37	3838.02	1.942434	0.000005	10.71	0.67	12.577	0.067
Si II	1304.37	3838.25	1.942610	0.000002	6.42	0.34	12.524	0.073
H I	1215.67	3843.06	2.161271	0.000015	25.23	2.12	13.041	0.032
C IV	1548.20	3843.81	1.482769	0.000003	5.16	0.83	13.087	0.069
C IV	1548.20	3844.08	1.482942	0.000019	18.61	4.30	13.167	0.084
C IV	1548.20	3844.75	1.483374	0.000004	21.58	0.76	13.817	0.013
C IV	1550.77	3850.20	1.482769	0.000003	5.16	0.83	13.087	0.069
C IV	1550.77	3850.47	1.482942	0.000019	18.61	4.30	13.167	0.084
C IV	1550.77	3851.14	1.483374	0.000004	21.58	0.76	13.817	0.013
H I	1215.67	3854.62	2.170781	0.000004	21.92	0.52	13.861	0.015
H I	1215.67	3862.53	2.177281	0.000027	42.92	3.52	13.025	0.031
H I	1215.67	3869.87	2.183320	0.000012	28.99	1.54	13.111	0.020
H I	1215.67	3873.43	2.186253	0.000017	38.66	2.26	13.143	0.022
H I	1215.67	3874.89	2.187449	0.000014	22.33	1.89	12.849	0.031
H I	1215.67	3878.93	2.190779	0.000012	25.59	1.58	12.988	0.023
H I	1215.67	3881.21	2.192647	0.000005	24.94	0.62	13.453	0.010
H I	1215.67	3883.18	2.194270	0.000005	22.14	0.64	13.350	0.012
H I	1215.67	3887.91	2.198162	0.000003	43.99	1.01	13.738	0.011
H I	1215.67	3889.30	2.199303	0.000056	42.93	11.88	12.716	0.207
H I	1215.67	3891.44	2.201069	0.000048	159.01	50.56	13.389	0.118
H I	1215.67	3893.52	2.202775	0.000004	41.08	0.75	14.064	0.011
H I	1215.67	3894.74	2.203777	0.000007	22.66	1.05	13.318	0.023
H I	1215.67	3896.55	2.205269	0.000064	108.28	8.44	13.826	0.041
H I	1215.67	3898.99	2.207278	0.000037	64.71	22.18	13.133	0.525
H I	1215.67	3899.56	2.207746	0.000494	115.62	17.23	13.489	0.297
C II	1334.53	3904.44	1.925698	0.000017	22.53	2.37	12.788	0.081
C II	1334.53	3904.80	1.925971	0.000003	10.32	0.37	13.124	0.031
H I	1215.67	3908.28	2.214920	0.000027	27.31	3.60	12.614	0.048
H I	1215.67	3909.86	2.216218	0.000003	25.14	0.35	13.905	0.009
H I	1215.67	3915.65	2.220982	0.000008	19.71	1.35	13.372	0.041
H I	1215.67	3916.44	2.221628	0.000013	63.12	1.21	14.080	0.011
H I	1215.67	3918.87	2.223629	0.000022	44.80	2.80	13.266	0.026
H I	1215.67	3919.46	2.224118	0.000009	10.04	1.75	12.536	0.082
C II	1334.53	3926.16	1.941975	0.000003	17.57	0.64	13.165	0.025
C II	1334.53	3926.77	1.942434	0.000005	16.38	0.67	13.482	0.028
C II	1334.53	3927.01	1.942610	0.000002	9.82	0.34	13.631	0.019
Ca II	3934.78	3934.77	-0.000003	0.000001	8.42	0.41	12.223	0.016
H I	1215.67	3935.92	2.237659	0.000011	31.74	1.40	13.147	0.016
H I	1215.67	3947.50	2.247180	0.000030	46.97	3.97	12.890	0.031
Mg II	2796.35	3954.77	0.414261	0.000001	7.31	0.18	12.809	0.011
N V	1238.82	3960.71	2.197161	0.000026	32.51	4.06	13.122	0.048
N V	1238.82	3961.95	2.198162	0.000003	31.46	0.58	14.568	0.026
Mg II	2803.53	3964.92	0.414261	0.000001	7.31	0.18	12.809	0.011
N V	1238.82	3965.55	2.201069	0.000048	96.15	7.61	13.580	0.041
Ca II	3969.59	3969.58	-0.000003	0.000001	8.42	0.41	12.223	0.016
N V	1238.82	3970.75	2.205269	0.000064	101.12	6.88	14.361	0.094
N V	1238.82	3973.24	2.207278	0.000037	58.75	7.26	13.779	0.135
N V	1242.80	3973.43	2.197161	0.000026	32.51	4.06	13.122	0.048
N V	1238.82	3973.82	2.207746	0.000494	193.86	129.48	13.992	0.596
N V	1242.80	3974.68	2.198162	0.000003	31.46	0.58	14.568	0.026
N V	1238.82	3976.65	2.210034	0.001863	221.92	201.82	13.708	0.847
N V	1242.80	3978.29	2.201069	0.000048	96.15	7.61	13.580	0.041
N V	1242.80	3983.51	2.205269	0.000064	101.12	6.88	14.361	0.094
N V	1242.80	3986.01	2.207278	0.000037	58.75	7.26	13.779	0.135
N V	1242.80	3986.58	2.207746	0.000494	193.86	129.48	13.992	0.596

Table 2. Absorption line parameter list

ID	λ_{rest}	λ_{obs}	z	σ_z	b	σ_b	LogN	σ_{LogN}
N V	1242.80	3989.43	2.210034	0.001863	221.92	201.82	13.708	0.847
Si IV	1393.76	3996.57	1.867485	0.000002	6.07	0.27	12.905	0.015
Si IV	1393.76	3996.93	1.867745	0.000004	5.38	0.67	12.373	0.033
Si IV	1393.76	3999.52	1.869598	0.000040	10.39	4.48	12.167	0.206
Si IV	1393.76	3999.75	1.869762	0.000003	7.07	0.53	13.122	0.028
Si IV	1393.76	4000.15	1.870055	0.000008	8.46	2.22	12.523	0.183
Si IV	1393.76	4000.32	1.870175	0.000066	23.00	5.09	12.643	0.174
Si IV	1393.76	4000.88	1.870576	0.000006	5.03	1.20	12.118	0.062
Si IV	1393.76	4001.58	1.871076	0.000003	9.97	0.48	12.833	0.017
Si IV	1393.76	4002.60	1.871813	0.000010	8.08	1.73	12.112	0.070
C IV	1548.20	4010.66	1.590541	0.000003	4.62	0.82	13.002	0.060
C IV	1548.20	4010.79	1.590621	0.000007	18.82	0.80	13.440	0.026
C IV	1550.77	4017.33	1.590541	0.000003	4.62	0.82	13.002	0.060
C IV	1550.77	4017.46	1.590621	0.000007	18.82	0.80	13.440	0.026
Si IV	1402.77	4022.42	1.867485	0.000002	6.07	0.27	12.905	0.015
Si IV	1402.77	4022.79	1.867745	0.000004	5.38	0.67	12.373	0.033
Si IV	1402.77	4025.39	1.869598	0.000040	10.39	4.48	12.167	0.206
Si IV	1402.77	4025.62	1.869762	0.000003	7.07	0.53	13.122	0.028
Si IV	1402.77	4026.03	1.870055	0.000008	8.46	2.22	12.523	0.183
Si IV	1402.77	4026.20	1.870175	0.000066	23.00	5.09	12.643	0.174
Si IV	1402.77	4026.76	1.870576	0.000006	5.03	1.20	12.118	0.062
Si IV	1402.77	4027.46	1.871076	0.000003	9.97	0.48	12.833	0.017
Si IV	1402.77	4028.49	1.871813	0.000010	8.08	1.73	12.112	0.070
Si IV	1393.76	4077.71	1.925698	0.000017	14.73	2.37	12.318	0.059
Si IV	1393.76	4078.09	1.925971	0.000003	6.75	0.37	12.775	0.021
Si IV	1393.76	4100.39	1.941975	0.000003	11.49	0.64	13.040	0.016
Si IV	1393.76	4101.03	1.942434	0.000005	10.71	0.67	13.426	0.023
Si IV	1393.76	4101.28	1.942610	0.000002	6.42	0.34	13.341	0.030
Si IV	1402.77	4104.08	1.925698	0.000017	14.73	2.37	12.318	0.059
Si IV	1402.77	4104.46	1.925971	0.000003	6.75	0.37	12.775	0.021
Si IV	1402.77	4126.91	1.941975	0.000003	11.49	0.64	13.040	0.016
Si IV	1402.77	4127.56	1.942434	0.000005	10.71	0.67	13.426	0.023
Si IV	1402.77	4127.81	1.942610	0.000002	6.42	0.34	13.341	0.030
C IV	1548.20	4309.48	1.783553	0.000024	29.66	4.14	13.051	0.060
C IV	1548.20	4313.52	1.786161	0.000004	23.43	0.57	13.915	0.011
C IV	1548.20	4314.57	1.786841	0.000009	6.12	1.69	12.572	0.077
C IV	1548.20	4315.13	1.787201	0.000004	8.03	0.65	13.169	0.027
C IV	1550.77	4316.65	1.783553	0.000024	29.66	4.14	13.051	0.060
C IV	1550.77	4320.69	1.786161	0.000004	23.43	0.57	13.915	0.011
C IV	1550.77	4321.75	1.786841	0.000009	6.12	1.69	12.572	0.077
C IV	1550.77	4322.31	1.787201	0.000004	8.03	0.65	13.169	0.027
??	1215.67	4390.66	2.611718	0.000036	20.77	4.32	13.063	0.082

heavy element lines, or simply noise features. Indeed all of these lines have column densities $\log N < 13.5$, close to the local detection limit. There is no observed correlation between the Doppler widths and column densities of the lines.

4.2 The Intervening Heavy Element Systems

A total of 78 heavy element lines have been fitted from eight intervening, and two associated heavy element systems. One further line was observed at 4390.66Å, right at the red end of the spectrum. It is not associated with any known heavy element system, and is possibly either C IV λ 1548 at redshift $z = 1.836$, or Mg II λ 2796 at redshift $z = 0.570$, although other identifications are possible. The profile fit was performed with the assumption that the line has the rest wavelength and oscillator strength of Ly α .

4.2.1 $z = 0.0000$

Narrow Ca II $\lambda\lambda$ 3934, 3969 is seen from the interstellar medium in the Galaxy.

4.2.2 $z = 0.4143$

A single Mg II $\lambda\lambda$ 2796, 2803 doublet occurs at this redshift, with Doppler parameter $b = 7 \text{ km s}^{-1}$ and column density $\log N(\text{Mg II}) = 13.1$.

4.2.3 $z = 1.483$

A complex of three C IV $\lambda\lambda$ 1548, 1550 doublets, spanning 75 km s^{-1} , is seen within the Ly α forest. Although the C IV complex is observed in the Ly α forest, and has no further confirming heavy element lines, the system has a distinctive pattern that makes this a firm identification.

4.2.4 Not $z = 1.5034$

Savaglio (1998) reported the tentative identification of a Mg II doublet at $z = 1.5034$. However, no corresponding Ly α absorption line is seen in the STIS data and no C IV absorption is visible in our spectrum, making the original identification very insecure.

4.2.5 $z = 1.591$

A C IV $\lambda\lambda 1548, 1550$ feature, consisting 2 lines separated by 9 km s^{-1} was seen at 4011 and 4018 Å, redward of the Ly α emission line. No Si IV absorption was detected for this system; $\log N(\text{Si IV}) < 12.3$ is a 4σ upper limit to the column density.

4.2.6 $z = 1.786$

Sealey et al. (1998) first reported C IV associated with a prominent Ly α line in the STIS data. Savaglio (1998) detected the C IV absorption at high resolution, but very low S/N. Mg I $\lambda\lambda 2852$ was also detected. The UCLES spectrum shows four C IV $\lambda\lambda 1548, 1550$ components spanning almost 400 km s^{-1} . Any Si IV $\lambda\lambda 1393, 1402$ absorption for this system, if significant, was blended with Ly α lines in the forest, making it impossible to determine a reliable column density.

4.2.7 $z = 1.87$

This heavy element system has a complex structure of nine Si IV $\lambda\lambda 1393, 1402$ components, spanning 450 km s^{-1} . Savaglio (1998) detected complex C IV absorption for this system, but noted that much higher S/N would be required to deblend the lines. She also detected Mg I $\lambda 2853$, but the identification of this line (normally only seen in damped Ly α systems) is doubtful.

4.2.8 $z = 1.925$

The UCLES spectrum shows a large saturated Ly α line, fitted by three components, at 3560 Å. Without the constraint of higher order Lyman series absorption lines, the column density for this system is very poorly constrained. C II $\lambda 1334$, Si III $\lambda 1206$, and Si IV $\lambda\lambda 1393, 1402$ absorption lines were detected for this system. 2 heavy element components were seen, at $z = 1.9256$ and $z = 1.9259$. This is over 100 km s^{-1} blueward of the centre of the saturated Ly α line; however no heavy element absorption was detected for the central hydrogen component.

Sealey et al. (1998) investigated this system as a possible cause of the Lyman break seen in the STIS spectrum at $\lambda \sim 2700$, concluding however that the system at $z = 1.942$ is more likely to be the major contributor. Savaglio (1998) searched for heavy element lines associated with this system in the EMMI spectrum, finding no associated C IV absorption, and only an upper limit to the column density of $\log N(\text{C IV}) < 13.7$. This implies that the column density ratios $\text{Si IV} / \text{C IV} \gtrsim 0.15$, and $\text{C II} / \text{C IV} \gtrsim 0.4$, both of which are relatively high (Songaila 1998). Savaglio tentatively identified Fe I $\lambda 2484$ and Fe II $\lambda 2382$ in the EMMI spectrum. Further investigation of the spectrum at the exact redshift of

the observed heavy element lines shows that these identifications are doubtful.

4.2.9 $z = 1.942$

The Ly α line is present in the UCLES spectrum (at 3577 Å), but it is saturated, and too noisy to determine an accurate column density directly. If solely responsible for the Lyman break seen in the STIS spectrum, however, this system has a column density of $\log N(\text{H I}) \sim 17.5$. C II $\lambda 1334$, Si II $\lambda\lambda 1260, 1304$, Si III $\lambda 1206$, and Si IV $\lambda\lambda 1393, 1402$ were all detected in the spectrum, and three components were fitted, at $z = 1.94197$, $z = 1.94243$, and $z = 1.94261$. No O I $\lambda 1302$ absorption was detected; a 4σ upper limit to the O I column density is $\log N(\text{O I}) < 12.95$.

Sealey et al. suggested that this system may be a good candidate for a measurement of the D / H ratio. Unfortunately, the weak $z = 1.94197$ line lies 60 km s^{-1} blueward of the other two stronger lines, and the hydrogen cloud associated with this line will probably adversely affect any determination of the deuterium abundance from the main system.

Savaglio (1998) identified strong C IV $\lambda\lambda 1548, 1550$ absorption at the same redshift as the absorption features in the UCLES data. Mg II $\lambda\lambda 2796, 2803$, and Al III $\lambda\lambda 1854, 1862$ were also detected for the strongest component.

4.2.10 $z = 2.077$

This heavy element system, identified by Savaglio (1998), has a weak C IV $\lambda\lambda 1548, 1550$ doublet. The corresponding Ly α line is seen at $z = 2.07717$ and has a log column density of 15.4. No associated heavy element lines were found in the UCLES spectrum, and a 4σ upper limit to the Si IV column density is $\log N(\text{Si IV}) < 11.9$.

4.3 The Associated Heavy Element Systems

The UCLES spectrum shows the clear signature of strong, broad N V absorption in the region $3960 < \lambda < 3990$ Å. The corresponding H I absorption, at $3885 < \lambda < 3900$ Å, is also broad, and apparently not saturated, indicative of highly ionized systems.

4.3.1 $z = 2.198$

A strong N V $\lambda\lambda 1238, 1242$ doublet, and corresponding Ly α line are seen at $z = 2.198$. The N V doublet ratio is roughly 1:1, yet the lines have residual intensity ~ 35 per cent of the continuum. The likely explanation for this is that there is incomplete coverage of the background source, as has been seen in other objects (see Barlow & Sargent 1997; Hamann et al. 1997). The Ly α and N V lines are consistent with near zero coverage of the emission line gas, and complete coverage of the continuum, implying the cloud is larger than the continuum but smaller than the emission line region. Another possibility is that the absorption lines arise in several regions which are sufficiently cool that they are unresolved, saturated, and distributed over $\sim 80 \text{ km s}^{-1}$ in velocity space so that at the instrument resolution used here the profile is

relatively smooth. We have not explored this far, but the conditions required for this to work at all for both H I and N V look somewhat contrived.

Savaglio (1998) observed the C IV absorption for this system. It was noted that the equivalent width ratio for the C IV doublet was lower than expected, further evidence for incomplete coverage of the source. The C IV emission line is much weaker than the Ly α emission line and the depth of the C IV absorption lines require that the continuum is not completely covered. Therefore the absorption is shared between continuum and emission line. Assuming all absorption for all ions involved comes from the same region uniformly and there is no velocity-dependent or ion-dependent emission line region geometry, the best-fit covering factors are 50 per cent of the continuum source, and 75 per cent of the emission line region. This result is partly based on the low S/N EMMI spectrum, and further observations of the C IV, Si IV and O VI absorption features are required to clarify the picture.

4.3.2 $z = 2.207$

A blend of very broad (Doppler parameter $b \sim 200 \text{ km s}^{-1}$) absorption lines, both for N V $\lambda\lambda 1238, 1242$ and Ly α , were fitted for this system. The fit was complicated by uncertainty in the precise shape of the Ly α & N V emission line continuum over the broad absorption feature, together with uncertainty in the covering factor. Also, the N V $\lambda 1242$ line from the $z = 2.198$ system lay on top of the N V $\lambda 1238$ line from the $z = 2.207$ system. We attempted to measure the covering factor, but no constraint was possible, so we assumed it to be 100 per cent. In order to obtain a satisfactory fit, however, we had to correct the continuum by subtracting a Gaussian centred on 3983 Å with FWHM = 670 km s^{-1} , and maximum depth 19 per cent of the original continuum level.

5 DISCUSSION

Perhaps the most important enhancement of the HDF-S project over its predecessor is the inclusion of the STIS instrument observations of the field containing the $z = 2.24$ QSO J2233-606. The STIS spectrograph will provide a high resolution (10 km s^{-1}) UV ($\lambda < 3500 \text{ Å}$) spectrum of the QSO. Furthermore, deep UV, optical and infra-red imaging of the STIS and surrounding flanking fields from both the HST and VLT observations will provide morphologies of galaxies near the QSO, and allow the accurate determination of photometric redshifts over the full range in absorber redshifts seen in the QSO spectrum.

One of the main aims of this project is to investigate the relationship between QSO absorbers and high redshift galaxies. The ground-based observations of the HDF-S QSO spectrum, reported here, and by Sealey et al. (1998) and Savaglio (1998), complement the STIS spectrum and are crucial to determining the properties of the intervening QSO absorbers and their association to galaxies seen in the STIS and flanking field images. In this paper we have reported eight heavy-element absorption systems which are potentially associated with galaxies. Combining this information with the imaging will allow investigation of the relationship

between heavy element abundances and galaxy type, environment and impact parameter.

An associated absorption system of this quasar shows evidence for incomplete coverage of both the emission-line region and the continuum source. Further data are required to establish whether or not the coverage is ion dependent, as it is in other such cases (e.g. Hamann et al. 1997).

ACKNOWLEDGEMENTS

The observations were obtained with the Anglo-Australian Telescope. We thank S. Savaglio and H. Ferguson for making the EMMI and STIS data available. Much of the data reduction and analysis was performed on the Starlink-supported computer network at the Institute of Astronomy. P. Outram acknowledges support from PPARC.

REFERENCES

- Abraham R. G., Tanvir N. R., Santiago B. X., Ellis R. S., Glazebrook K., van den Bergh S., 1996, MNRAS, 279, L47
- Barlow T.A., Sargent W.L.W., AJ, 113, 136
- Boyle B. J., 1997, AAO Newsletter, 83, 4
- Carswell R. F., Webb J. K., Cooke A. J., Irwin M. J., 1992, VPFIT Manual (program and manual available from rfc@ast.cam.ac.uk)
- Hamann F., Barlow T.A., Junkkarinen V., Burbidge E.M., 1997, ApJ, 478, 80
- Kirkman D., Tytler D., 1997, ApJ, 489, 123
- Lanzetta K. M., Bowen D. V., Tytler D., Webb J. K., 1995, ApJ, 442, 538
- Lu L., Sargent W. L. W., Womble D. S., Takada-Hidai M., 1996, ApJ, 472, 509
- Madau P., Ferguson H. C., Dickinson M. E., Giavalisco M., Steidel C. C., Fruchter A., 1996, MNRAS, 283, 1388
- Outram P. J., Chaffee F. H., Carswell R. F., 1998 (in preparation)
- Savaglio S., 1998, AJ (accepted)
- Sealey K. M., Drinkwater M. J., Webb J. K., 1998, ApJ, 499, L135
- Songaila A., 1998, AJ, 115, 2184
- Steidel C. C., Giavalisco M., Dickinson M., Adelberger K. L., 1996, AJ, 112, 352
- Webb J. K., 1987, Ph.D. thesis, Cambridge University
- Williams R. E. et al., 1996, AJ, 112, 1335